Polymer Chemistry

RSC Publishing

PAPER

View Article Online
View Journal | View Issue

Cite this: *Polym. Chem.*, 2013, **4**, 1132

Thiophene spacers impart crystallinity and enhance the efficiency of benzotrithiophene-based conjugated polymers for bulk heterojunction photovoltaics

Shang-Che Lan, Po-An Yang, Meng-Jie Zhu, Chia-Min Yu, Jian-Ming Jiang and Kung-Hwa Wei*

In this study we synthesized the donor–acceptor conjugated copolymers **PBTT4BT** and **PBTT4BO** featuring benzotrithiophene (**BTT**) units as donors and benzothiadiazole (**BT**) and benzoxadiazole (**BO**) units, respectively, as acceptors, linked through 4-dodecylthiophene spacers. The presence of the spacer units enhanced not only the solubility of the synthesized polymers but also their molecular packing in the solid state; both of these polymers exhibited good crystallinity, as evidenced by a *d*-spacing of 23.8 Å in the (100) plane in their X-ray diffraction curves. When we used these synthesized polymers in bulk heterojunction photovoltaic device applications, the optimal device incorporating **PBTT4BO**/**PC$_{61}$BM** as the active layer exhibited a low efficiency of 3.2%, due to the poor solubility of **PBTT4BO**, whereas the optimal device incorporating the more-soluble **PBTT4BT** and **PC$_{71}$BM** displayed an efficiency of 4.4%, which is substantially 1.5% higher than that for the **PBTTBT**/**PC$_{71}$BM** device, where **PBTTBT** was formed by copolymerizing **BTT** and **BT** units without any spacer. After thermal annealing, the efficiency of the **PBTT4BT**/**PC$_{71}$BM** device improved further to 5.6%, with a V_{OC} value of 0.72 V, a J_{SC} value of 11.58 mA cm^{-2} and a fill factor of 67%. The annealed **PBTT4BT**/**PC$_{71}$BM** active layer possessed a nanoscaled network-like morphology with rod-like **PBTT4BT** domains that were beneficial for charge separation and transport; accordingly, the power conversion efficiency of the annealed **PBTT4BT**/**PC$_{71}$BM** photovoltaic device was enhanced greatly over that of the as-cast **PBTT4BT**/**PC$_{71}$BM** device.

Received 3rd October 2012
Accepted 8th November 2012

DOI: 10.1039/c2py20819a

www.rsc.org/polymers

Introduction

Polymer solar cells (PSCs) have attracted a great deal of attention because of their low cost, light weight, flexibility, and ease of fabrication relative to silicon-based solar cells.[1–3] Bulk heterojunctions (BHJs), in which a conjugated polymer as a p-type material is blended with a fullerene derivative (*e.g.*, **PC$_{61}$BM**) as an n-type material, are the most successful active layer structures for PSCs. Recently, the power conversion efficiencies (PCEs) of some conjugated polymer-based BHJ devices have reached over 7% without the need to adopt new device architecture.[4] Ideally, the polymer in the active layer should have a broad absorption spectrum to absorb more photons, high hole mobility to transport carriers, and a suitable energy level offset with respect to the fullerenes to afford a high open-circuit voltage (V_{OC}).

The rational design and synthesis of low-band gap conjugated polymers remains an important aspect of the quest for PSCs with high PCEs. The donor–acceptor (D/A) copolymer approach, where electron donor and electron acceptor units are copolymerized, is an effective means of obtaining conjugated polymeric materials exhibiting low band gaps as well as suitable energy level offsets with respect to the fullerenes.[5] D/A polymers featuring a weak donor and a strong acceptor have displayed the ideal energy level offset with respect to fullerenes.[6] Indeed, copolymerizing a weakly electron donating benzodithiophene unit[6,7] with a variety of strongly electron accepting units, such as thieno[3,4-*b*]thiophene,[1c] fluorinated benzo[1,2,5]thiadiazole (**BT**),[4c] benzo[1,2,5]oxadiazole (**BO**),[8] and thieno[3,4-*c*]pyrrole-4,6-dione,[9] has resulted in BHJ devices exhibiting PCEs ranging from 5 to 7%.

Another important feature of an ideal conjugated polymer is crystallinity, because crystalline polymers not only have better resistance to moisture and oxygen permeation, which result in longer device life time but also typically lead to higher hole mobilities. A case in point is poly(3-hexylthiophene) (P3HT), which can form highly crystalline states and nanoscaled bicontinuous networks with fullerenes upon thermal annealing in the active layer of BHJ devices, thereby providing quite-decent PCEs (4% or more), even though P3HT has a simple molecular structure.[10] It is, however, difficult to predict *a priori* which molecular structures will result in crystalline polymers, even though some general directions (*e.g.*, planarity,[11] regioregularity) can be followed; notably, most D/A copolymers are

Department of Materials Science and Engineering, National Chiao Tung University, 1001 Ta Hsueh Road, Hsinchu, 30050, Taiwan, ROC. E-mail: khwei@mail.nctu.edu.tw; Fax: +886-3-5724727; Tel: +886-3-5731771

amorphous materials. Only some specific monomer units, including thieno[3,2-*b*]thiophene,[12] dithieno[3,2-*b*:2′,3′-*d*]silole,[13] and thieno[3,4-*c*]pyrrole-4,6-dione,[14] have exhibited the potential to form crystalline polymers.

Recently, a new planar donor, benzotrithiophene (**BTT**), was designed for the synthesis of a series of **BTT**-based copolymers for organic electronic device applications.[15] The electron donating ability of **BTT** is slightly stronger than that of benzodithiophene; although it has an asymmetric structure, the copolymers of **BTT** and thiophene exhibited good crystallinity and high mobility, making them suitable for use in organic thin film transistors. Moreover, **BTT** has been copolymerized with benzo[1,2,5]thiadiazole (**BT**) to form a copolymer that has been used to fabricate BHJ solar cells exhibiting a PCE of 2.2%. This limited efficiency was due to the highly phase-separated active layer morphology, presumably because of the polymer's low solubility or miscibility.

In this present study, we wished to further improve the solubility of D/A copolymers incorporating **BTT** units and also enhance their crystallinity. It has been reported that D/A polymers featuring 4-alkylthiophene units as spacers between the D and A units can not only exhibit greater solubility[16] but also enhance the crystalline potential because of low steric demand on the planarity of the conjugated backbone when using 4-alkylthiophene.[17] Here, we employed 4-dodecylthiophene as a spacer between **BTT** and **BT** monomer units to improve the solubility of their copolymer and to induce crystallinity in the copolymer. The presence of the thiophene-based spacer would, however, slightly elevate the energy level of the highest occupied molecular orbital (HOMO) of the polymer, relative to that of the corresponding polymer lacking the thiophene spacer, and, therefore, decrease the value of V_{OC} of the resulting photovoltaic device. Accordingly, we also tested the effects of another acceptor, **BO**, because it has electron-withdrawing ability similar to that of **BT**, meanwhile it is more electronegative than **BT** and could maintain the HOMO energy level.[8,12b,18]

Experimental

Materials and synthesis

Unless stated otherwise, all reagents were purchased from chemical suppliers (Aldrich, Alfa, Acros, *etc.*) and used without further purification. All solvents were dried using appropriate agent(s) under purged N_2 prior to use. 5-(1-Octylnonyl)benzo[1,2-*b*:3,4-*b*′:5,6-*d*″]trithiophene(**1**),[15b] 2,5-dibromo-benzo[1,2,5]oxadiazole (**2**),[18] 2-trimethylstannyl-4-dodecylthiophene,[16] and 4,7-bis(5-bromo-4-dodecyl-thien-2-yl)benzo[1,2,5]thiadiazole (**M3**)[16] were synthesized according to literature procedures.

5-(1-Octylnonyl)-2,8-bis(trimethylstannyl)benzo[1,2-*b*:3,4-*b*′:5,6-*d*″]trithiophene (**M1**). A two-neck round-bottom flask containing **1** (300 mg, 0.62 mmol) was evacuated and filled with N_2 three times and then anhydrous tetrahydrofuran (THF, 20 mL) was added. *tert*-Butyllithium (1.7 M in pentane, 1.3 mL, 2.2 mmol) was added drop wise into the flask at −78 °C and then the mixture was warmed to room temperature and stirred for a further 3 h. The reaction mixture was cooled to −78 °C again, trimethyltinchloride (1 M in hexane, 2.5 mL, 2.5 mmol) was added, and then the mixture was warmed to room temperature overnight. The reaction was quenched through the addition of water; the mixture was extracted with hexane (3 × 100 mL) and then the combined organic phases were dried ($MgSO_4$) and concentrated. The crude product was washed alternately with triethylamine and hexane to afford a yellow viscous liquid (382 mg, 76%). ^{1}H NMR (300 MHz, $CDCl_3$): δ (ppm) 7.78 (s, 1H), 7.62 (s, 1H), 7.46 (s, 1H), 2.97 (m, 1H), 1.71 (m, 6H), 1.26–1.22 (m, 24H), 0.852 (t, $J = 13.2$ Hz, 6H), 0.48 (s, 18H). ^{13}C NMR (300 MHz, $CDCl_3$): δ (ppm) 149.68, 138.74, 137.67, 135.40, 134.41, 133.28, 132.49, 131.94, 130.55, 130.00, 129.90, 42.41, 38.11, 31.85, 29.64, 29.48, 29.28, 27.54, 22.63, 14.10.

4,7-Bis(4-dodecyl-thien-2-yl)benzo[1,2,5]oxadiazole (**3**). A two-neckround-bottom flask containing 2,5-dibromobenzo[1,2,5]oxadiazole (**2**, 3.00 g, 10.9 mmol), 2-trimethylstannyl-4-dodecylthiophene (10.4 g, 25.0 mmol), and tetrakis-(triphenylphosphine)palladium(0) [$Pd(PPh_3)_4$, 606 mg, 0.52 mmol] was purged with N_2 for 20 min to remove O_2. Anhydrous THF (30 mL) was added and then the mixture was heated under reflux. After 24 h, the mixture was cooled to room temperature and concentrated using a rotary evaporator. The crude product was purified through column chromatography (SiO_2; EtOAc–hexanes, 5 : 95) to give an orange solid (5.61 g, 83%). ^{1}H NMR (300 MHz, $CDCl_3$): δ (ppm) 7.95 (d, $J = 1.2$ Hz, 2H), 7.549 (s, 2H), 7.01 (d, 0.9 Hz, 2H), 2.66 (t, $J = 15.3$ Hz, 4H), 1.68 (m, 4H), 1.33–1.25 (m, 36H), 0.875 (t, $J = 13.2$ Hz, 6H). ^{13}C NMR (300 MHz, $CDCl_3$): δ (ppm) 147.84, 145.05, 137.54, 130.16, 126.07, 122.06, 121.64, 31.92, 30.61, 30.45, 29.67, 29.62, 29.47, 29.36, 22.70, 14.13.

4,7-Bis(5-bromo-4-dodecylthien-2-yl)benzo[1,2,5] oxadiazole (**M2**). *N*-Bromosuccinimide (NBS, 3.10 g, 17.4 mmol) was added in portions to a stirred solution of **3** (5.00 g, 8.05 mmol) in dimethyl formamide (DMF, 40 mL) and then the mixture was stirred in the dark at room temperature for 8 h. Brine was added and then the aqueous phase was extracted with ether (3 × 200 mL). The combined organic phases were washed twice with brine, dried ($MgSO_4$), and concentrated. The residue was purified through column chromatography (SiO_2; CH_2Cl_2–hexanes, 10 : 90) to give an orange solid (5.62 g, 90%). ^{1}H NMR (300 MHz, $CDCl_3$): δ (ppm) 7.71 (s, 2H), 7.24 (s, 2H), 2.59 (4H, $J = 15.6$ Hz), 1.63 (m, 4H), 1.31–1.236 (m, 36H), 0.853 (t, $J = 13.5$ Hz, 6H). ^{13}C NMR (300 MHz, $CDCl_3$): δ (ppm) 147.47, 144.01, 137.10, 129.75, 125.73, 121.40, 111.57, 31.92, 29.67, 29.58, 29.40, 29.36, 29.25, 22.69, 14.13.

PBTT4BO. A solution of **M1** (70 mg, 0.086 mmol) and **M2** (67 mg, 0.086 mmol) in anhydrous toluene was purged with N_2 for 20 min to remove O_2. $Pd(PPh_3)_4$ (9.9 mg, 10 mmol%) was added and then the solution was heated at 100 °C. After 48 h, an end-capping agent 2-(tributylstannyl)thiophene (100 μL) was added; 4 h later, another end-capping agent, 2-bromothiophene (100 μL), was added and then the mixture was heated overnight. The temperature was lowered to 50 °C and the mixture was then added dropwise into stirred MeOH (40 mL). The precipitated polymer was filtered off. The solid was placed in a Soxhlet extractor and washed sequentially with acetone, hexane, and chloroform (CF). The CF solution was re-precipitated in MeOH to obtain the final polymer (70 mg, 66%). Anal. calcd: C, 74.08; H, 9.12; N, 2.30. Found: C, 73.66; H, 8.92; N, 1.98%.

PBTT4BT. Following the procedure described previously, the reaction of **M1** (70 mg, 0.086 mmol) and **M3** (68 mg, 0.086 mmol) in the presence of tri-*o*-tolylphosphine [P(*o*-tol)$_3$, 2.1 mg, 8.0 mol%] and tris(dibenzylideneacetone) dipalladium (Pd_2dba_3, 1.6 mg, 2 mol%) provided the copolymer **PBTT4BT** (76 mg, 72%). Anal. calcd: C, 73.11; H, 9.00; N, 2.27. Found: C, 73.33; H, 9.22; N, 2.61%.

PBTTBT. Following the procedure described previously, the reaction of **M1** (70 mg, 0.086 mmol) and **M3** (25.2 mg, 0.086 mmol) in the presence of tri-*o*-tolylphosphine [P(*o*-tol)$_3$, 2.1 mg, 8.0 mol%] and tris(dibenzylideneacetone) dipalladium (Pd_2dba_3, 1.6 mg, 2 mol%) provided the copolymer **PBTT4BT** (26 mg, 50%). Anal. calcd: C, 67.91; H, 6.84; N, 4.53. Found: C, 67.32; H, 6.92; N, 4.88%.

Measurements and characterization

^{1}H NMR spectra of solutions in $CDCl_3$ were recorded using a Varian UNITY-300 spectrometer. Chemical shifts are reported relative to the solvent signal. Mass spectra were recorded using a Micromass TRIO-2000 spectrometer. Thermogravimetric analysis (TGA) was performed using a TA Instruments Q500 apparatus operated at a heating rate of 20 °C min^{-1} under a N_2 flow. The number- and weight-average molecular weights of the polymers were determined through size exclusion chromatography (SEC) using a Waters 1515 system, polystyrene standards, and THF as the eluent; the temperature of the system was set at 45 °C. UV-Vis absorption spectra were recorded using a Hitachi U-4100 spectrophotometer. Solution UV-Vis absorption spectra were recorded from 10^{-5} M solutions in toluene. Polymer thin films were spin-coated from toluene solutions (1 mg mL^{-1}) onto a quartz substrate. Cyclic voltammetry (CV) was performed using a BAS 100 electrochemical analyzer operated at a scan rate of 50 mV s^{-1}. A three-electrode cell was used, with tetrabutylammoniumhexafluorophosphate ($TBAPF_6$, 0.1 M in MeCN) as the supporting electrolyte, a glassy carbon electrode as the working electrode, a Pt wire as the counter electrode, and Ag/$AgNO_3$ (0.01 M in MeCN) as the reference electrode. The ferrocene/ferrocenium ion (Fc/Fc^+) pair was used as the internal standard with the assumption that the energy level of Fc is 4.8 eV below vacuum. X-ray diffraction (XRD) patterns were recorded using a Bruker D8 high-resolution X-ray diffractometer operated in grazing incidence mode. Samples were prepared by drop-casting a solution of the polymer in toluene (1 mg mL^{-1}) onto a silicon wafer. Topographic and phase images of the active layers (surface area: 5 × 5 μm^2) were obtained using a Digital Nanoscope III atomic force microscope operated in the tapping mode under ambient conditions. The thickness of the active layer of the device was measured using a Veeco Dektak 150 surface profiler. Transmission electron microscopy (TEM) images were recorded using an FEI T12 transmission electron microscope; a low-energy electron beam (120 keV) provided sufficient contrast to distinguish the polymer-rich and fullerene-rich regions of the active layer in all of the samples without the need for heavy ion staining.

Fabrication and measurement of photovoltaic cells

The photovoltaic cells had the configuration glass/indium tin oxide (ITO)/poly(3,4-ethylenedioxythiophene):polystyrenesulfonate (PEDOT:PSS)/polymer:fullerene/Ca/Al. ITO-coated glass was pre-cleaned with detergent, DI water, acetone, and isopropanol in an ultrasonication bath (10 min each step) and then exposed to UV/ozone for 20 min. PEDOT:PSS was spin-cast onto the substrate and then annealed at 150 °C for 20 min in air. The active layer was spin-cast onto the PEDOT:PSS layer in a glove box, and then dried under N_2. To prepare the **PBTT4BO** cell, **PBTT4BO** (2 mg) and the fullerene (3 mg) were dissolved in CF (500 μL) at 60 °C; for the **PBTT4BT** cell, the polymer (6 mg) and the fullerene (9 mg) were dissolved in *o*-dichlorobenzene (DCB, 500 μL) at 80 °C; for the **PBTTBT** cell, the polymer (2 mg) and the fullerene (4 mg) were dissolved in chlorobenzene (CB, 300 μL) at 80 °C. Ca (20 nm) and Al (100 nm), thermally deposited under vacuum, were used as the counter electrode. Each device featured four cells; the effective layer area of each cell was 0.04 cm^2. Annealing was performed by heating cells at a specific temperature for 20 min prior to deposition of the cathode.

The photovoltaic characteristics were measured using a Keithley 2400 source meter under simulated AM 1.5G illumination at 100 mW cm^{-2}; a Xe lamp-based Newport 66902150 W solar simulator with an AM1.5G filter was used as the white light source. A silica photodiode (Hamamatsu S1133) was employed as a standard to confirm the light intensity.

Results and discussion

Synthesis and thermal characteristics

Scheme 1 displays the synthesis of the **BTT** donor (**M1**) and the **BT** and **BO** acceptor units (**M2** and **M3**, respectively); they were all prepared with slight modifications of literature procedures.[14a,15,18] We performed the copolymerizations of these D and A units using the Stille cross-coupling method (Scheme 2); **PBTT4BT** was synthesized using a catalysis system containing Pd_2dba_3 and P(*o*-tol). The alkyl chains attached to the spacer and D units provided **PBTT4BT** with good solubility in DCB, CF, and THF, resulting in a decent molecular weight (M_n = 20 kDa; PDI = 9.0). **PBTT4BO** would have precipitated during polymerization when using Pd_2dba_3 and P(*o*-tol) as the catalyst system; therefore, we used a relatively weaker catalyst [$Pd(PPh_3)_4$] for its

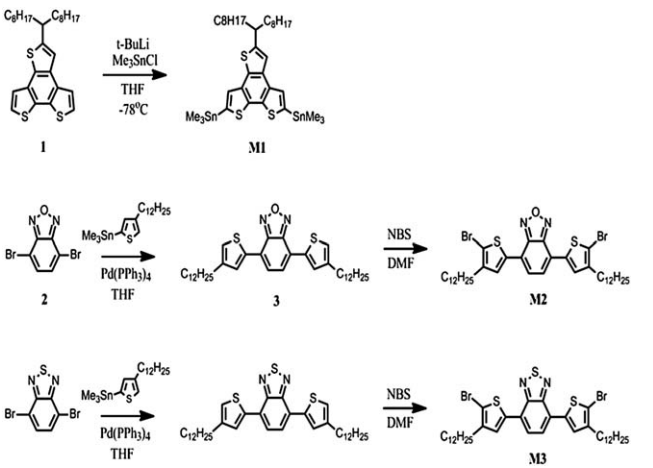

Scheme 1 Synthesis and structures of monomers.

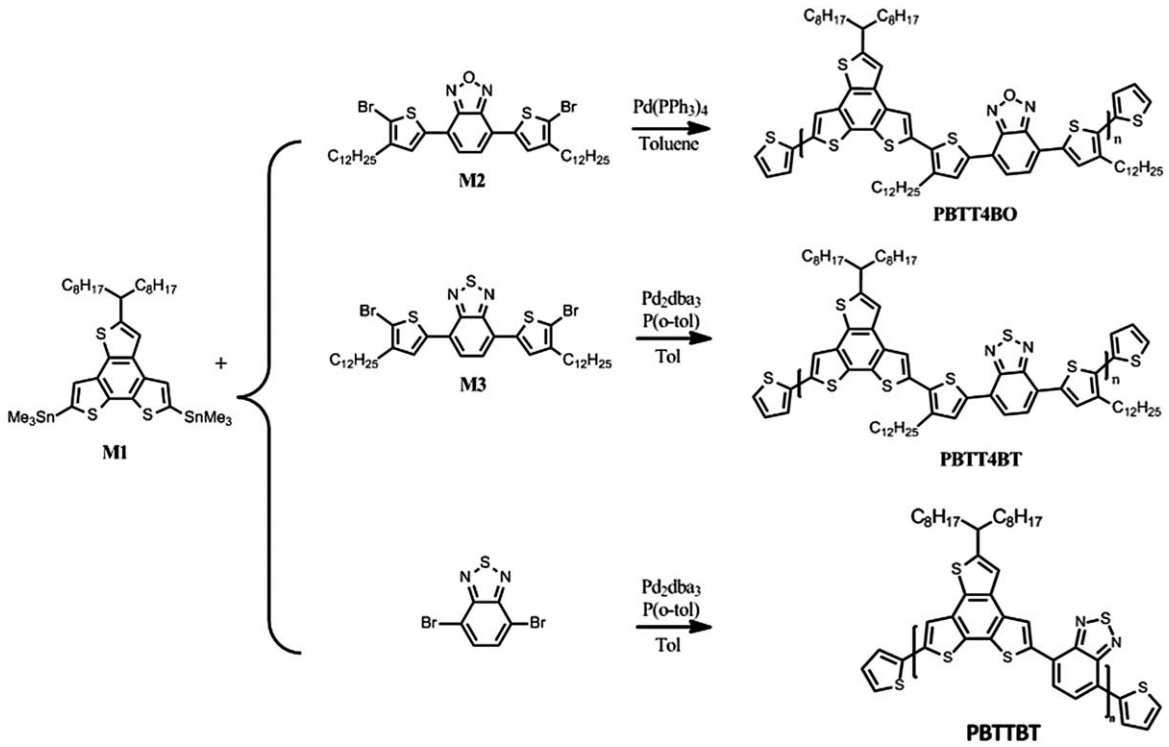

Scheme 2 Synthesis and structures of the polymers **PBTT4BO**, **PBTT4BT** and **PBTTBT**.

polymerization. Nevertheless, **PBTT4BO** still exhibited poor solubility and could be dissolved only in toluene and CF. The portion of **PBTT4BO** soluble in THF was used for SEC analysis, providing a molecular weight of 6 kDa and a PDI of 6.2. These two polymers also exhibited good thermal stability, each with a thermal degradation temperature (at 5% weight loss) higher than 350 °C. Of the two polymers, **PBTT4BO** had the lower decomposition temperature, probably because of its lower molecular weight and the greater ring strain of its oxadiazole rings. Table 1 summarizes the GPC and TGA data of the two polymers.

Optical properties

Fig. 1 displays normalized UV-Vis absorption spectra of diluted solutions of the polymers in toluene and of their thin films; Table 2 summarizes the numerical data. In solution, **PBTT4BT** and **PBTT4BO** provided similar absorption profiles, with absorption peaks near 350, 600, and 700 nm. The peak located near 600 nm was due to internal charge transfer (ICT) from the D to the A; the peak located near 700 nm was the vibronic peak attributable to π–π interactions between polymer chains. The vibronic peaks for the **PBTT4BT** and **PBTT4BO** films were more intense in the solid state than in solution, presumably because of stronger π–π interactions in the solid films. The optical bandgaps, which we calculated from the onsets of the spectrum profiles for the thin films, for **PBTT4BO** and **PBTT4BT** were 1.63 and 1.64 eV, respectively. These nearly identical bandgaps suggest that **BT** and **BO** have roughly similar electron-withdrawing abilities.

Table 1 Molecular weights and thermal properties of the polymers

Polymer	M_n[a] (kDa)	M_w[a] (kDa)	PDI[a]	T_d[b] (°C)
PBTT4BO	6744	41 659	6.2	354
PBTT4BT	20 465	184 591	9.0	395
PBTTBT	7081	8710	1.2	—

[a] Values of M_n, M_w, and PDI of the polymers were determined through SEC (polystyrene standards; THF). [b] 5%-Weight-loss temperatures in N_2.

Electrochemical properties

We used CV to determine the energy levels of the HOMOs and the lowest unoccupied molecular orbitals (LUMOs) of the conjugated polymers. Fig. 2 presents the onset oxidation and reduction potentials with respect to Fc/Fc^+; both polymers underwent quasi-reversible oxidation processes and reversible reduction processes. The HOMO and LUMO energy levels for **PBTT4BO** were −5.32 and −3.58 eV, respectively; for **PBTT4BT** they were −5.24 and −3.59 eV, respectively. The band gap energies of **PBTT4BT** determined using CV are in close agreement with their optical band gap energies deduced from their UV-Vis absorption spectra, whereas the CV band gap was slightly larger than the optical band gap in the case of **PBTT4BO**. The HOMO energy level of **PBTT4BO** was lower than that of **PBTT4BT**, due to the oxygen atom being more electronegative than a sulfur atom; as a result, **PBTT4BO** had a larger energy level offset with respect to the fullerene.

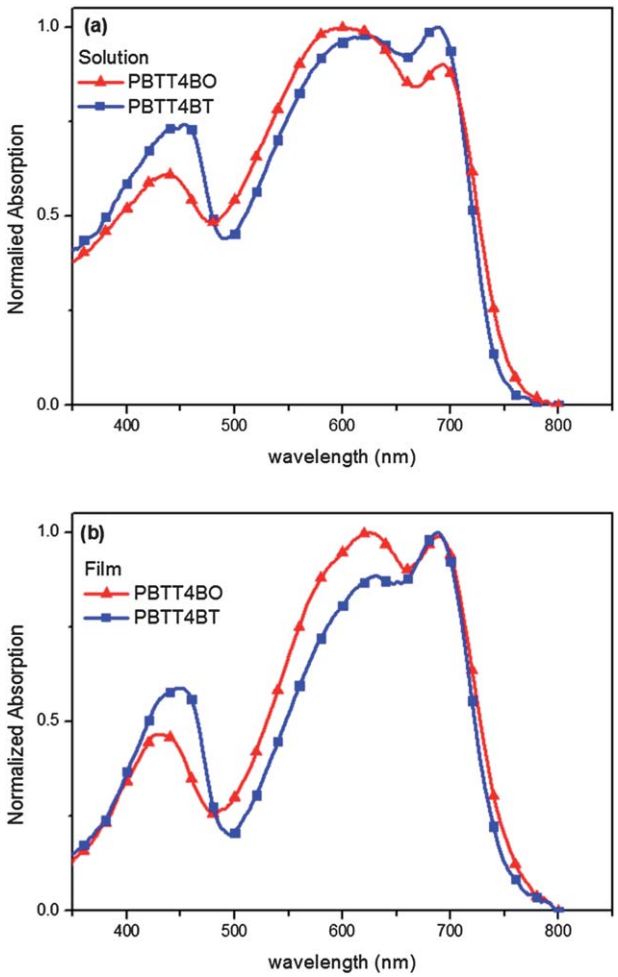

Fig. 1 UV-Vis absorption spectra of the polymers **PBTT4BO** and **PBTT4BT** (a) in dilute toluene solution (1×10^{-5} M) and (b) as solid films.

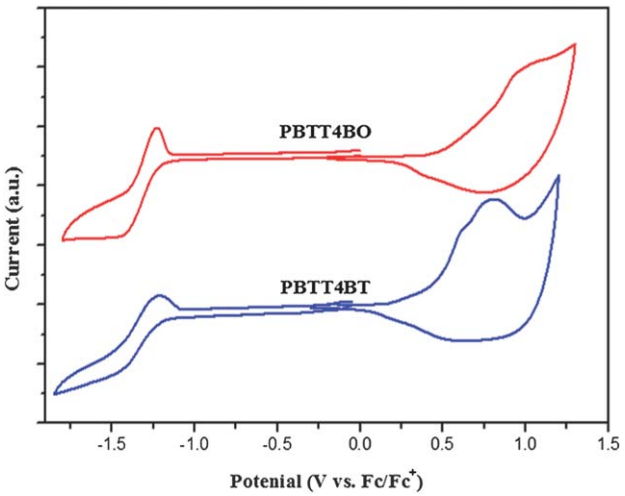

Fig. 2 Cyclic voltammograms of the polymers **PBTT4BO** and **PBTT4BT** as solid films.

Computational study

Due to different band gap correlations for **PBTT4BO** and **PBTT4BO** in optical and electrochemical properties, the computational analyses were performed to obtain the relationship between band gap and energy levels of **PBTT4BO** and **PBTT4BT**. Quantum-chemical calculations were based on the method of density functional theory (DFT) at the B3LYP/6-31G* level. To simplify the calculation, only three repeat units were taken, with which alkyl chains were replaced by methyl groups. Fig. 3 displays the calculated electron density distributions and the energy levels of HOMOs and LUMOs for **BTT4BO** and **BTT4BT**. Both of the polymers show similar electron density distributions; the electron density of HOMO was distributed along the backbone of polymers with the electron density of LUMO mainly located at the acceptor unit. The correlation of calculated band gap energies for **BTT4BO** and **BTT4BT** (1.94 *vs.* 1.91 eV) is in agreement with the observation of the UV-Vis spectrum (1.63 *vs.* 1.64 eV).

The theoretical calculation indicated that both the LUMO and HOMO energy levels of **BTT4BO** are deeper than those of **BTT4BT**, which is partly in agreement with the CV experiments where the HOMO of **BTT4BO** is deeper than that of

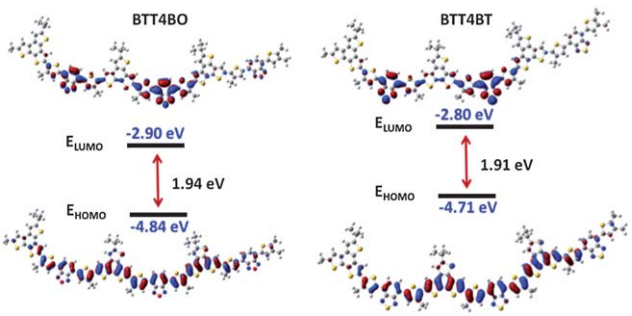

Fig. 3 Theoretically calculated HOMOs and LUMOs of **BTT4BO** and **BTT4BT** at the B3LYP/6-31G* level.

Table 2 Optical and electrochemical properties of **PBTT4BO** and **PBTT4BT**

Polymer	λ_{max} (nm) (in CF)	λ_{max} (nm) (film)	λ_{onset} (nm) (film)	$E_g^{opt\ a}$ (eV)	HOMO^b (eV)	LUMO^b (eV)	$E_g^{EC\ c}$ (eV)
PBTT4BO	600	626 684	766	1.63	−5.32	−3.58	1.74
PBTT4BT	690	690	768	1.64	−5.24	−3.59	1.65

[a] Optical bandgap calculated from the absorption onset in the film. [b] HOMO and LUMO energy levels determined using the equations HOMO = $-(4.8 + E^{ox})$ eV and LUMO = $-(4.8 + E^{red})$ eV. [c] Electrochemical bandgap calculated from LUMO − HOMO.

BTT4BT, and the LUMOs for **BTT4BO** and **BTT4BT** are identical. This difference in the LUMOs determined from the theoretical calculations and CV measurement is probably due to the fact that the LUMO of conjugated polymers is difficult to be accurately measured in the CV experiment.

XRD analysis and molecular packing

To investigate the molecular packing of **PBTT4BO** and **PBTT4BT** in the solid state, we performed XRD analyses of their as-cast thin films that we had drop-cast from toluene solutions onto silica substrates and after annealing at 150 °C for 20 min. Fig. 4 displays the XRD patterns of the as-cast and annealed polymer films. For the as-cast **PBTT4BT** film, the only reflection peak appeared at a 2θ value of 3.7°, corresponding to edge-on lamellar stacking in the (100) plane with a *d*-spacing of 23.8 Å.[10c,19] After annealing, a higher-order reflection peak appeared at a 2θ value of 7.7°, arising from the (200) plane with a *d*-spacing of 11.6 Å, along with a more-intense (100) peak. Hence, the degree of crystallinity of **PBTT4BT** improved appreciably after thermal annealing. The chains of **PBTT4BT** predominantly adopted a layered structure with an edge-on orientation relative to the substrate; this structure would presumably assist charge carrier transport in the vertical direction.[20] Recently, it has been suggested that the curvature of a polymer backbone would greatly affect its stacking.[21] The less curvature in the polymer backbone results in more crystallinity in the polymer thin film. The **PBTT4BT** featured thiophene spacer has less curvature than **BTT** and **BT** copolymer without the spacer, as determined in our DFT simulations. Hence, **PBTT4BT** reveals crystallinity, whereas **BTT–BT** does not exhibit crystallinity as shown in Fig. 4. The **PBTT4BO** film displayed the same single reflection peak and tendency as that of **PBTT4BT**, however it lacked another higher-order reflection peak in the (200) plane, indicating that the tendency of **PBTT4BT** to crystallize was greater than that of **PBTT4BO**; a similar heteroatom effect is evident in, for example, the crystallinity of dithieno[3,2-*b*:2′,3′-*d*]siloleandcyclopenta[2,1-*b*:3,4-*b*′]dithiophene.[13] The larger size of the sulfur atom increases the spacing between the polymer chains and improves polymer reorganization. In addition, **PBTT4BO** is less soluble than **PBTT4BT**, resulting in faster precipitation after solvent evaporation and decreasing the amount of time available for self-organization.

Photovoltaic devices

We fabricated solar devices having the configuration glass/ITO/PEDOT:PSS/polymer:fullerene/Ca/Al. Fig. 5 displays the *J*–*V* curves of these devices under AM 1.5G conditions; Table 3 summarizes the photovoltaic parameters. Because of the low solubility of **PBTT4BO**, its active layer could be spin-coated only from CF, providing a layer thickness of approximately 100 nm. The PCE of the device incorporating **PBTT4BO** was higher when it was blended with **$PC_{61}BM$** than with **$PC_{71}BM$**, presumably because of greater phase separation in the active layer. The highest measured PCE for the as-cast **PBTT4BO**/**$PC_{61}BM$**-containing device was 2.9%, with a V_{OC} value of 0.75 V, a J_{SC} value of 7.14 mA cm^{-2}, and a fill factor (FF) of 54%; the average efficiency measured over 20 devices was 2.3%. We observed a slight improvement in performance for the device that had been subjected to annealing: values of V_{OC}, J_{SC}, and FF of 0.75 V, 7.54 mA cm^{-2}, and 55%, respectively, resulting in an efficiency of 3.2% (average efficiency for 20 devices: 2.7%).

Because **PBTT4BT** had better solubility in DCB, we used it as the processing solvent to prepare the active layer. The device incorporating the as-cast **PBTT4BT**/**$PC_{61}BM$** blend as the active layer exhibited a PCE of 3.9%, while that of the as-cast **PBTT4BT**/**$PC_{71}BM$** device was 4.4% with a V_{OC} value of 0.69 V, a J_{SC} value of 11 mA cm^{-2}, and an FF of 58%. The lower open-circuit voltage for this device is due to the higher HOMO energy level of **PBTT4BT** elevated by the thiophene spacer. Comparing to the BHJ device of **PBTTBT**, where **PBTTBT** was produced by copolymerization of **BTT** and **BT** units, the

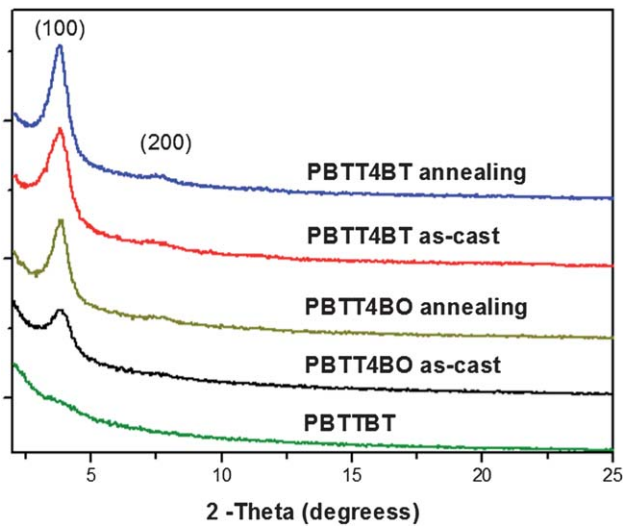

Fig. 4 XRD patterns of the pristine **PBTT4BO** and **PBTT4BT** films.

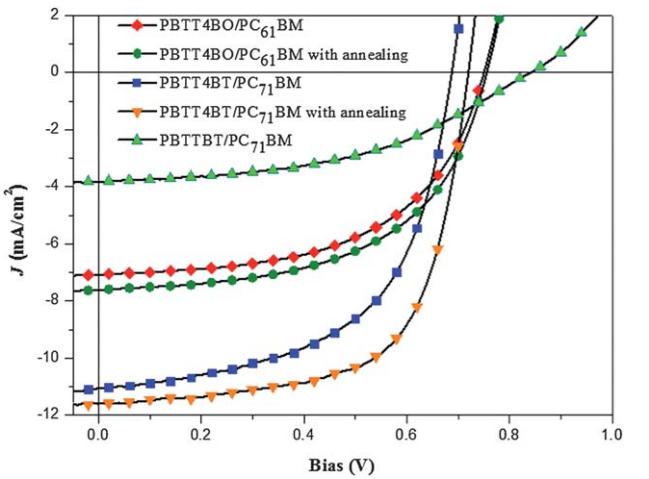

Fig. 5 *J*–*V* characteristics of optimal photovoltaic devices of **PBTT4BO** and **PBTT4BT** before and after heat treatment.

Table 3 Photovoltaic properties of **PBTT4BO** and **PBTT4BT** blends with fullerene derivatives

Active layer (polymer–fullerene = 1 : 1.5 wt%)	Annealing	V_{oc} (V)	J_{sc} (mA cm^{-2})	FF (%)	PCE (avg[a]) (%)	Thickness (nm)
PBTT4BO/PC$_{61}$BM	—	0.75	−7.14	54	2.9 (2.3)	117
PBTT4BO/PC$_{61}$BM	100 °C per 20 min	0.76	−7.54	55	3.2 (2.7)	108
PBTT4BO/PC$_{71}$BM	—	0.79	−3.17	57	1.4 (1.2)	75
PBTT4BT/PC$_{61}$BM	—	0.70	−8.90	62	3.9 (3.6)	90
PBTT4BT/PC$_{71}$BM	—	0.69	−10.98	58	4.4 (4.3)	85
PBTT4BT/PC$_{71}$BM	150 °C per 20 min	0.72	−11.58	67	5.6 (5.5)	97
PBTTBT/PC$_{71}$BM	—	0.84	−3.90	46	1.5 (1.2)	65

[a] Average PCE calculated from 20 cells.

efficiency of the BHJ **PBTT4BT** device improves greatly (4.4 *vs.* 1.5%), presumably due to the better solubility and the crystalline nature of **PBTT4BT** that gives better miscibility and charge mobility in the active layer. After thermal treatment at 150 °C for 20 min, the photovoltaic parameters for the **PBTT4BT/PC$_{71}$BM** device were all enhanced, with a V_{OC} value of 0.72 V, a J_{SC} value of 11.58 mA cm^{-2}, and an FF of 67%, resulting in a device efficiency of 5.6%.

Morphological analyses

Fig. 6 presents atomic force microscopy (AFM) images of various active layers incorporating **PBTT4BT** and **PBTT4BO**. Fig. 6(a) and (b) display the height and the phase image for the as-cast and the annealed films of **PBTT4BO/PC$_{61}$BM**, respectively. The phase images of both of these polymer films revealed phase-aggregation, with the thermally treated film featuring slightly rougher and slightly larger aggregated domains; this

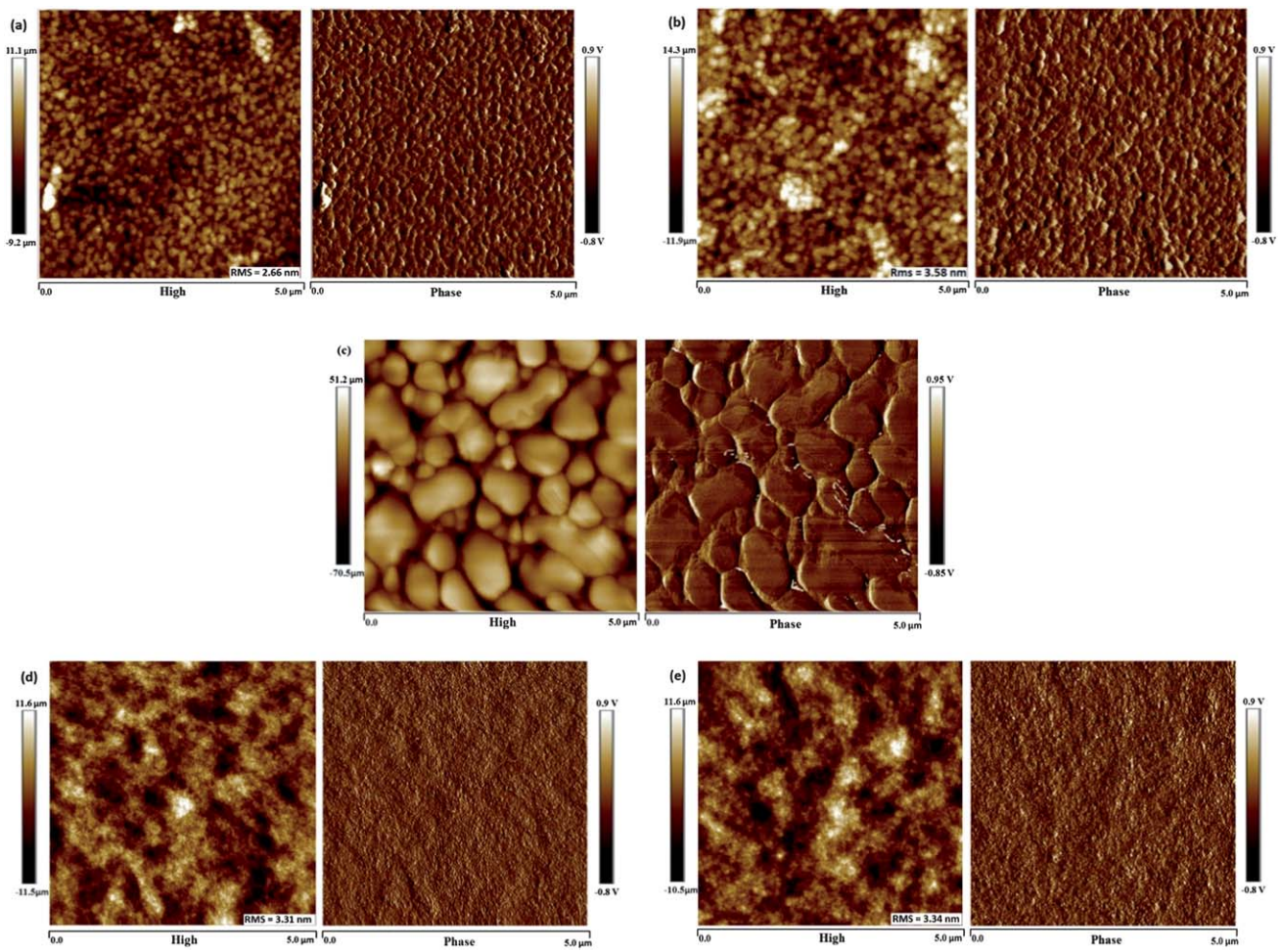

Fig. 6 AFM images of films of (a) as-cast **PBTT4BO/PC$_{61}$BM**, (b) annealed **PBTT4BO/PC$_{61}$BM**, (c) as-cast **PBTT4BO/PC$_{71}$BM**, (d) as-cast **PBTT4BT/PC$_{71}$BM**, and (e) annealed **PBTT4BT/PC$_{71}$BM**.

aggregation was probably due to the poor solubility of **PBTT4BO**. In both cases the diameters of aggregates were approximately150–200 nm. The aggregation became much more pronounced in the case of **PBTT4BO/PC$_{71}$BM** [Fig. 6(c)], consistent with the sharp drop in efficiency of the corresponding device. Fig. 6(e) and (f) reveal that the as-cast **PBTT4BT/PC$_{71}$BM** film was relatively homogeneous and remained so after thermal treatment, with the roughness in both cases being 3.3 nm, without any apparent aggregation. The PCE of the annealed **PBTT4BT/PC$_{71}$BM** device was, however, substantially improved over that of its as-cast device, indicating that AFM analysis of the surface morphology could not differentiate the actual morphology of the active layer.

Fig. 7 presents TEM images of the **PBTT4BO/PC$_{61}$BM** and **PBTT4BT/PC$_{71}$BM** films. The dark and bright regions in these images correspond to fullerene-rich and polymer-rich domains, respectively, due to the electron density of the fullerenes (density: *ca.* 1.5 g cm^{-3}) being higher than that of the polymers (density: *ca.* 1.1 g cm^{-3}).[22] Fig. 7(a) reveals that the diameter of each dark region in the **PBTT4BO/PC$_{61}$BM** film was approximately 50 nm; this domain size is too large to provide enough interfaces for exciton dissociation. After annealing, the phase-separation between the polymer and fullerene domains in the **PBTT4BO/PC$_{61}$BM** film was more complete [Fig. 7(b)], indicating that **PBTT4BO** had greater crystallinity; these domains provided better channels for charge transport, thereby improving the performance of the devices. Fig. 7(c) displays a rather uniform **PBTT4BT/PC$_{71}$BM** morphology that resulted because **PBTT4BT** and **PC$_{71}$BM** were mixed well in DCB. Fig. 7(d) reveals a network-like morphology in the annealed **PBTT4BT/PC$_{71}$BM** film, where **PBTT4BT** appeared as rod-like crystalline domains (width: *ca.* 5 nm) distributed in the fullerene matrix. This nanoscale phase separation in the annealed **PBTT4BT/PC$_{71}$BM** film appears to be optimal, producing a more than 25% enhancement in the PCE of the annealed device relative to that for the as-cast case (5.6 *vs.* 4.4%).

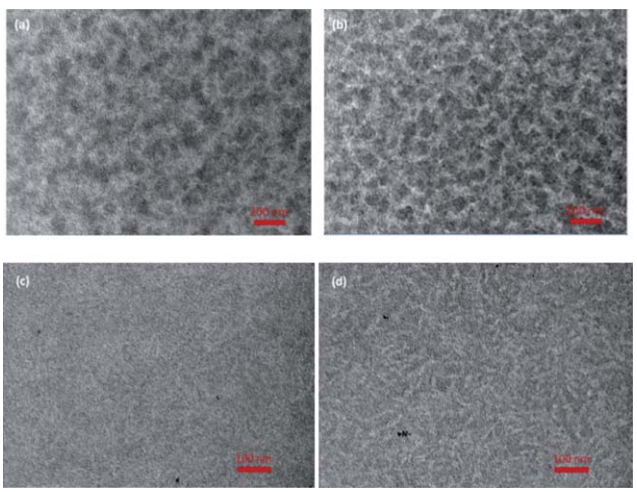

Fig. 7 TEM images of active layers of (a) as-cast **PBTT4BO/PC$_{61}$BM**, (b) annealed **PBTT4BO/PC$_{61}$BM**, (c) as-cast **PBTT4BT/PC$_{71}$BM**, and (d) annealed **PBTT4BT/PC$_{71}$BM**.

Conclusions

We have synthesized two new crystalline D/A polymers, **PBTT4BO** and **PBTT4BT**, that feature benzotrithiophene units as donor moieties and benzothiadiazole and benzoxadiazole units, respectively, as acceptor moieties, separated by 4-dodecylthiophene spacers. The HOMO and LUMO energy levels for **PBTT4BO** were −5.32 and −3.58 eV, respectively; for **PBTT4BT**, they were −5.24 and −3.59 eV, respectively, resulting in a band gap of approximately 1.63 eV. Both **PBTT4BO** and **PBTT4BT** formed edge-on lamellae that stacked in the (100) plane with a *d*-spacing of 23.8 Å, as evidenced from their XRD patterns. The degrees of crystallinity of **PBTT4BT** and **PBTT4BO** were improved appreciably after annealing at 150 °C for 20 min. The as-cast **PBTT4BT/PC$_{71}$BM** photovoltaic devices exhibited an optimal PCE of 4.4%, which is substantially higher than that of 1.5% for the **PBTTBT/PC$_{71}$BM** device, where **PBTTBT** was formed by copolymerizing **BTT** and **BT** units without any spacer. For the annealed **PBTT4BT/PC$_{71}$BM** photovoltaic devices, the PCE improved to 5.6%—an enhancement of more than 25% after annealing, presumably because **PBTT4BT** formed rod-like crystalline domains (width: *ca.* 5 nm) distributed in the fullerene matrix, as determined by transmission electron microscopy. Due to the poor solubility of **PBTT4BO** and its low molecular weight, the fabrication of the **PBTT4BO** into reasonable photovoltaic devices was severely limited. Therefore, the comparison of the photovoltaic performances of the **BTT4BO** and **BTT4BT** case reflects more on the device differences than on the molecular differences.

Acknowledgements

The authors thank Chia-Min Chen for assisting with the XRD and TEM analyses, and also thank the National Science Council, Taiwan, for financial support (NSC101-3113-P-009-005).

Notes and references

1 (*a*) G. Yu, J. Gao, J. C. Hummelen, F. Wudl and A. J. Heeger, *Science*, 1995, **270**, 1789–1791; (*b*) S. Günes, H. Neugebauer and N. S. Sariciftci, *Chem. Rev.*, 2007, **107**, 1324–1338; (*c*) H. Y. Chen, J. Hou, S. Zhang, Y. Liang, G. Yang, Y. Yang, Y. Yu, Y. Wu and G. Li, *Nat. Photonics*, 2009, **3**, 649–653.

2 (*a*) J. Alstrup, M. Jørgensen, A. J. Medford and F. C. Kerbs, *ACS Appl. Mater. Interfaces*, 2011, **3**, 4075–4084; (*b*) L. Yang, T. Zhang, H. Zhou, S. C. Price, B. J. Wiley and W. You, *ACS Appl. Mater. Interfaces*, 2011, **3**, 4075–4084.

3 (*a*) Y. Y. Lee, K. H. Tu, C. C. Yu, S. S. Li, J. Y. Hwang, C. C. Lin, K. H. Chen, L. C. Chen, H. L. Chen and C. W. Chen, *ACS Nano*, 2011, **5**, 6564–6570; (*b*) C. L. Hsu, C. T. Lin, J. H. Huang, C. W. Chu, K. H. Wei and L. J. Li, *ACS Nano*, 2012, **6**, 5031–5039.

4 (*a*) C. M. Amb, S. Chen, K. R. Graham, J. Subbiah, C. E. Small, F. So and J. R. Reynolds, *J. Am. Chem. Soc.*, 2011, **133**, 10062–10065; (*b*) S. M. Su, C. Y. Kuo, M. C. Yuan, U. S. Jeng, C. J. Su and K. H. Wei, *Adv. Mater.*, 2011, **23**, 3315–3319; (*c*) H. Zhou, L. Yang, A. C. Stuart, S. C. Price, S. Liu and W. You, *Angew.*

Chem., Int. Ed., 2011, **50**, 2995–2998; (*d*) L. Hou, S. Zhang, X. Guo, F. Xu, Y. Li and J. Hou, *Angew. Chem., Int. Ed.*, 2011, **50**, 9697–9702; (*e*) H. J. Son, W. Wang, T. Xu, Y. Liang, Y. Wu, G. Li and L. Yu, *J. Am. Chem. Soc.*, 2011, **133**, 1885–1894.

5 (*a*) J. Roncali, *Chem. Rev.*, 1997, **97**, 173–206; (*b*) C. Duan, F. Huang and Y. Cao, *J. Mater. Chem.*, 2012, **22**, 10416–10434; (*c*) H. J. Son, B. Carsten, H. I. Jung and L. Yu, *Energy Environ. Sci.*, 2012, **5**, 8158–8170; (*d*) Y. Li, *Acc. Chem. Res.*, 2012, **45**, 723–733; (*e*) C. U. Chen, C. M. Chen, D. Kekuda, S. C. Lan, C. W. Chu and K. H. Wei, *J. Polym. Sci., Part A: Polym. Chem.*, 2010, **48**, 1669–1675.

6 H. Zhou, L. Yang, S. Stonejing and W. You, *ACS Appl. Mater. Interfaces*, 2010, **2**, 1377–1383.

7 (*a*) J. Hou, M.-H. Park, S. Zhang, Y. Yao, L.-M. Chen, J.-H. Li and Y. Yang, *Macromolecules*, 2008, **41**, 6012–6018; (*b*) L. Huo and J. Hou, *Polym. Chem.*, 2011, **2**, 2453.

8 J. M. Jiang, P. A. Yang, H. C. Chen and K. H. Wei, *Chem. Commun.*, 2011, **47**, 8877–8879.

9 Y. Zou, A. Najari, P. Berrouard, S. Beaupré, R. B. Aïch, Y. Tao and M. Leclecc, *J. Am. Chem. Soc.*, 2010, **132**, 5330–5331.

10 (*a*) W. Ma, C. Yang, X. Gong, K. Lee and A. J. Heeger, *Adv. Funct. Mater.*, 2005, **15**, 1617–1622; (*b*) G. Li, V. Shrotriya, J. Huang, Y. Yao, T. Moriarty, K. Emery and Y. Yang, *Nat. Mater.*, 2005, **4**, 864–868; (*c*) M. Y. Chiu, U. S. Jeng, C. H. Su, K. S. Liang and K. H. Wei, *Adv. Mater.*, 2008, **20**, 2573–2578.

11 (*a*) H. H. Cho, T. E. Kang, K. H. Kim, H. Kang, H. J. Kim and B. J. Kim, *Macromolecules*, 2012, **45**, 6415–6423; (*b*) H. J. Park, Y. Lee, J. W. Jo and W. H. Jo, *Polym. Chem.*, 2012, **3**, 2928–2932; (*c*) J. Min, Z.-G. Zhang, S. Zhang and Y. Li, *Chem. Mater.*, 2012, **24**, 3247–3254.

12 (*a*) S. Subramaniyan, H. Xin, S. F. Kim and S. A. Jenekhe, *Macromolecules*, 2011, **44**, 6245–6248; (*b*) J. M. Jiang, P. A. Yang, H. C. Chen and K. H. Wei, *Macromolecules*, 2011, **44**, 9155–9163; (*c*) G. Y. Chen, Y. H. Chen, Y. J. Chou, M. S. Su, C. M. Chen and K. H. Wei, *Chem. Commun.*, 2011, **47**, 5064–5066.

13 H.-Y. Chen, J. Hou, A. E. Hayden, H. Yang, K. N. Houk and Y. Yang, *Adv. Mater.*, 2010, **22**, 371–375.

14 (*a*) M. C. Yuan, M. Y. Chiu, S. P. Liu, C. M. Chen and K. H. Wei, *Macromolecules*, 2010, **43**, 6936–6938; (*b*) C. Ottone, P. Berrouard, G. Louarn, S. Beaupr, D. Gendron, M. Zagorska, P. Rannou, A. Najari, S. Sadki, M. Leclerc and A. Pron, *Polym. Chem.*, 2012, **3**, 2355–2365; (*c*) J. Huang, Y. Zhao, W. He, H. Jia, Z. Lu, B. Jiang, C. Zhan, Q. Pei, Y. Liub and J. Yao, *Polym. Chem.*, 2012, **3**, 2832–2841.

15 (*a*) C. B. Nielsen, J. M. Fraser, B. C. Schroeder, J. Du, A. J. White, W. Zhang and I. McCulloch, *Org. Lett.*, 2011, **13**, 2414–2417; (*b*) B. C. Schroeder, C. B. Nielsen, Y. J. Kim, J. Smith, Z. Huang, J. Durrant, S. E. Watkins, K. Song, T. D. Anthopoulos and I. McCulloch, *Chem. Mater.*, 2011, **23**, 4025–4031; (*c*) C. B. Nielsen, B. C. Schroeder, A. Hadipour, B. P. Rand, S. E. Watkins and I. McCulloch, *J. Mater. Chem.*, 2011, **21**, 17642–17645; (*d*) C. B. Nielsen, R. S. Ashraf, B. C. Schroeder, P. D'Angelo, S. E. Watkins, K. Song, T. D. Anthopoulos and I. McCulloch, *Chem. Commun.*, 2012, **48**, 5831–5834.

16 H. Zhou, L. Yang, S. Xiao, S. Liu and S. W. You, *Macromolecules*, 2010, **43**, 811–820.

17 L. Yang, H. Zhou and W. You, *J. Phys. Chem. C*, 2010, **114**, 16793–16800.

18 (*a*) N. Blouin, A. Michaud, D. Gendron, S. Wakim, E. Blair, R. N. Plesu, M. Belletete, G. Durocher, Y. Tao and M. Leclerc, *J. Am. Chem. Soc.*, 2008, **130**, 732–742; (*b*) X. Wang, S. Chen, Y. Sun, M. Zhang, Y. Li, X. Li and H. Wang, *Polym. Chem.*, 2011, **2**, 2872.

19 (*a*) D. M. DeLongchamp, R. J. Kline, E. K. Lin, D. A. Fischer, L. J. Richter, L. A. Lucas, M. Heeney, I. McCulloch and J. E. Northrup, *Adv. Mater.*, 2007, **19**, 833–837; (*b*) E. Ahmed, S. Subramaniyan, F. S. Kim, H. Xin and S. A. Jenekhe, *Macromolecules*, 2011, **44**, 7207–7219.

20 I. Osaka, R. Zhang, G. Sauvé, D.-M. Smilgies, T. Kowalewski and R. D. McCullough, *J. Am. Chem. Soc.*, 2009, **131**, 2521–2529.

21 X. Guo, S. R. Puniredd, M. Baumgarten, W. Pisula and K. J. Müllen, *J. Am. Chem. Soc.*, 2012, **134**, 8404–8407.

22 C. W. T. Bulle-Lieuwma, W. J. H. van Gennip, J. K. J. van Duren, P. Jonkheijm, R. A. J. Janssen and J. W. Niemantsverdriet, *Appl. Surf. Sci.*, 2003, **203–204**, 547–549.

